Explaining Darwin's Corollary to Haldane's Rule: The Role of Mitonuclear Interactions in Asymmetric Postzygotic Isolation Among Toads

Yaniv Brandvain,*,[1] Gregory B. Pauly,[†] Michael R. May,* and Michael Turelli*,[2]
*Department of Evolution and Ecology, University of California, Davis, California 95616 and [†]Natural History Museum of Los Angeles County, Los Angeles, California 90007

ABSTRACT We examine the basis of Darwin's corollary to Haldane's rule, which describes viability and fertility differences between F_1 produced from reciprocal crosses. We analyzed asymmetries in hybrid viability from >100 reciprocal crosses involving 36 toad species to test whether relatively high rates of mitochondrial *vs.* nuclear evolution produce dams with systematically less viable F_1 hybrid progeny. We find no such effect, suggesting a predominant role for stochastic accumulation of asymmetric epistatic incompatibilities.

AS Darwin (1859, Chap. 8) noted, interspecific reciprocal crosses often differ in whether fertilization occurs and in the viability and fecundity of F_1 hybrids. Even under optimal laboratory conditions, reciprocal F_1s often show viability or fecundity differences. This pattern of asymmetric intrinsic postzygotic isolation has been dubbed "Darwin's corollary to Haldane's rule" (Turelli and Moyle 2007). While asymmetric fertilization success can be produced under autosomal genetic control, Darwin's corollary requires deleterious epistatic interactions (*i.e.*, Dobzhansky–Muller incompatibilities, DMIs) involving uniparentally inherited factors such as mitochondria, sex chromosomes, epigenetic programming, or maternal effects (Turelli and Moyle 2007), because only uniparentally inherited factors will differentially affect F_1 produced from reciprocal crosses.

Turelli and Moyle (2007) contrasted deterministic *vs.* stochastic explanations for Darwin's corollary, depending on whether the cross that produces less fit hybrids is predictable from relative rates of evolution for uniparentally *vs.* biparentally inherited factors. Differences in the relative rates of evolution can lead to different expected fitnesses from reciprocal crosses. Consider the species pair A–B. If the proportion of mitochondrial to nuclear substitutions in lineage A exceeds that in lineage B, we expect more mitonuclear DMIs in AB F_1 hybrids with A mothers *vs.* BA hybrids with B mothers, simply because there are more potential incompatibilities in the AB cross than in the BA cross. Thus, if mitonuclear DMIs contribute significantly to lowered interpopulation (Burton *et al.* 2006; Ellison and Burton 2008; Montooth *et al.* 2010; Meiklejohn *et al.* 2013) or interspecific (*e.g.*, Fishman and Willis 2006; Lee *et al.* 2008; Chou *et al.* 2010; Rieseberg and Blackman 2010) fitness, as often argued (*e.g.*, Rand *et al.* 2004; Gershoni *et al.* 2009; Chou and Leu 2010; Lane 2011; Burton and Barreto 2012), directional asymmetry may be predictable from relative rates of mitochondrial *vs.* nuclear evolution.

Turelli and Moyle (2007) conjectured that the deterministic signal associated with directional effects produced by a particular class of DMIs (*e.g.*, mitonuclear incompatibilities) was likely to be overwhelmed by both stochastic effects and other classes of asymmetric incompatibilities. The theoretical analyses pioneered by Orr (1993) describe the accumulation of DMIs as rare—independent and inherently stochastic—events associated with molecular differences between diverging taxa. Different realizations of these stochastic processes will produce different outcomes. Thus, even when the expected number of DMIs between reciprocal crosses is equal (corresponding to equal numbers of nuclear and mitochondrial substitutions), the actual number and/or effects of DMIs will typically differ because of the stochasticity inherent in the emergence of DMIs

doi: 10.1534/genetics.113.161133
Manuscript received December 30, 2013; accepted for publication March 17, 2014; published Early Online April 1, 2014.
Supporting information is available online at http://www.genetics.org/lookup/suppl/doi:10.1534/genetics.113.161133/-/DC1.
[1]Present address: Department of Plant Biology, University of Minnesota, St. Paul, Minnesota 55108.
[2]Corresponding author: 1 Shields Ave., University of California, Davis, CA 95616. E-mail: mturelli@ucdavis.edu

from interspecific differences (Orr 1993; Turelli and Moyle 2007).

Despite these caveats, in the first investigation of deterministic asymmetry effects, Bolnick *et al.* (2008) found a weak but statistically significant signal associated with mitochondrial *vs.* nuclear evolution in centrarchid fishes. For 13 of 18 reciprocal crosses in their study (72%), viability was lower when the species with the relatively greater ratio of mtDNA to nuclear substitutions was used as the maternal parent. This observation is consistent with the deterministic asymmetry hypothesis, but was somewhat surprising in light of the relatively small effect expected with plausible parameters for mitonuclear contributions to hybrid inviability. Here we examine whether this deterministic pattern holds using more extensive data from another clade, toads of the genus *Bufo* (taxonomy following Pauly *et al.* 2009, which maintains consistency with the names used in Malone and Fontenot 2008). We describe patterns of asymmetry produced at different stages of F_1 formation and development and at different levels of phylogenetic divergence.

We examine the success of Blair's (1972) experimental crosses as summarized by Malone and Fontenot (2008) across three stages of toad development: fertilization, hatching, and metamorphosis. These stages differ in whether mitonuclear incompatibilities can plausibly explain observed asymmetries:

1. *Fertilization* (measured as the proportion of eggs fertilized): Fertilization can depend on sperm–egg incompatibilities (*e.g.*, Vacquier and Swanson 2011), but is very unlikely to reflect F_1 mitonuclear DMIs as envisioned in the deterministic theory. Hence, fertilization informs the tempo of asymmetric reproductive isolation, but is a negative control for the importance of mitonuclear DMIs.
2. *Hatching* (measured as the proportion of fertilized eggs that hatched): Hatching of fertilized eggs involves interactions between alleles in the F_1 as well as interactions between the F_1 embryo and maternal contributions to the egg; it therefore compounds offspring genotype with another uniparental factor (maternal effects) that may swamp the signal of deterministic effects associated with mitonuclear incompatibilities.
3. *Metamorphosis* (measured as the proportion of larvae metamorphosed): The period from hatching to metamorphosis completes the maternal–zygotic transition (Wang and Dey 2006). It provides the best case for testing the deterministic effects of mitonuclear incompatibilities.

Testing the deterministic theory requires estimates of mitochondrial and nuclear branch lengths on a shared topology. We performed phylogenetic analyses for each gene region using MrBayes 3.2 (Ronquist *et al.* 2012) to identify substitution models for each locus (one mitochondrial and five nuclear loci; see *Methods* in Supporting Information File S1, Table S1, Table S2, Figure S1, Figure S2, Figure S3, Figure S4, Figure S5, Figure S6, Figure S7, Figure S8, and Figure S9). To generate

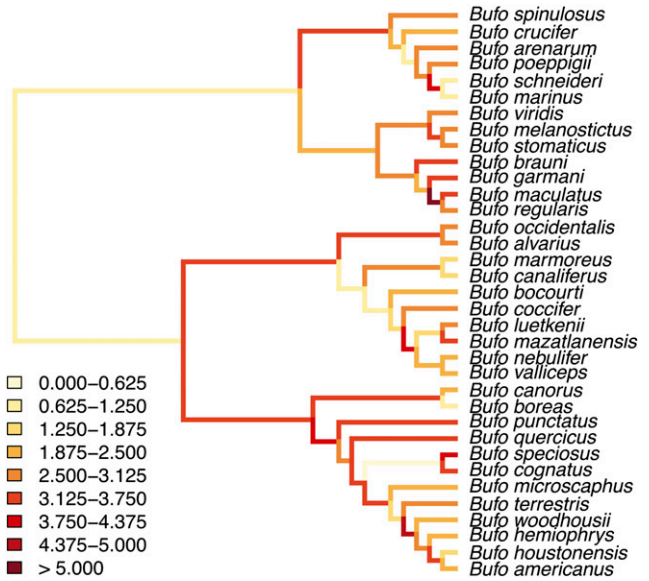

Figure 1 The majority-rule consensus tree for the genus *Bufo*. Branch lengths are relative to time on an ultrametric tree. Branch colors represent the relative amount of mitochondrial to nuclear evolution [log(mitochondrial branch length/nuclear branch length)] as indicated by the legend (estimated using MrBayes 3.2; Ronquist *et al.* 2012). We estimated the expected amount of evolution for each branch under the topological constraint described in the text with MrBayes 3.2 by unlinking nuclear and mitochondrial branch lengths to estimate mitonuclear asymmetry on a shared topology. We estimated relative divergence times using BEAST (Drummond *et al.* 2012). Data were gathered from GenBank with additional sequencing to complete the data matrix (accession numbers, primers, alignments, additional descriptions of our methods, and code for tree generation and computing relative branch lengths are presented in File S1, Table S1 and Table S2; File S2, alignments; and File S3, code). Statistical analyses were performed in R (R Development Core Team 2008).

a shared mitonuclear topology for our analysis (*i.e.*, a species tree), we constrained the topology of our combined nuclear–mitochondrial analysis on the deeper clade relationships evident in the nuclear trees (Figure 1), allowing us to accommodate an apparent mitochondrial introgression event that caused a deep discordance between nuclear and mitochondrial gene trees (see Methods and Results in Supporting Information File S1 and Figure S10). The resulting species tree is highly supported (*i.e.*, high clade posterior probabilities; see Figure S11) and provides estimates of mitonuclear substitution rate asymmetry (see Figure S12 and Figure S13). Excluding crosses spanning the mitochondrial capture event does not alter our qualitative results (not shown).

Figure 2 displays the tempo of evolution of asymmetric reproductive isolation, for both the raw data small light blue dots and thin light blue lines in Figure 2) and the node-weighted averages (Fitzpatrick 2002; dark blue squares and thick lines in Figure 2). Not surprisingly, asymmetries are found in fertilization success (Figure 2A) and through development (Figure 2, B and C) across all levels of divergence. We test the deterministic theory by asking whether taxa with higher relative mitochondrial-to-nuclear substitution rates

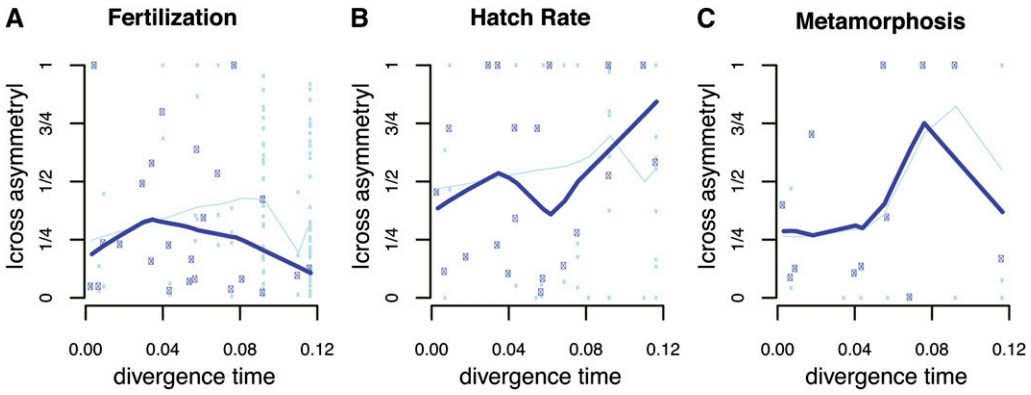

Figure 2 Reciprocal-cross asymmetry across fertilization and through development. The *x*-axis represents ultrametric distance between two nodes (Figure 1). The relative difference in reciprocal cross success is $\rho = (A \times B - B \times A)/(A \times B + B \times A)$. The *y*-axis represents the absolute value of ρ. The entire data set is presented with light blue points, and the thin light blue line displays local smoothing by lowess (R Development Core Team 2008). Dark blue boxes and thick lines present node-weighted average values that correct for phylogenetic nonindependence (Fitzpatrick 2002). Developmental stages are: (A) Fertilization, (B) hatching, and (C) metamorphosis.

(see the definition of δ_A in Figure 3) are more likely to be worse dams in a reciprocal cross (Figure 3). We find no support for this prediction. Rather, we observe a trend in the other direction across all developmental stages. This result is robust to uncertainty in tree topology and branch lengths; for a large majority of trees sampled from the posterior, across all developmental stages, the relationship between relative mitochondrial to nuclear substitution rates and reciprocal cross asymmetry trended against the prediction of the deterministic theory (Figure 3). In fact, aside from one chance observation in our negative control (fertilization), none of the 2000 (nonindependent) tests (1000 trees × 2 measures [hatching and metamorphosis]) provided statistically significant support for the deterministic theory (Figure 3).

Thus, reciprocal–cross asymmetry, while pervasive across toad development, is not driven by the deterministic effects of mitonuclear incompatibilities, at least as estimated from relative rates of mitochondrial *vs.* nuclear evolution. Although theoretical analysis predicted a very weak effect (Turelli and Moyle 2007), Bolnick *et al.* (2008) found tentative support for the deterministic prediction using molecular data comparable to ours. Specifically, 13 of 18 reciprocal crosses reported by Bolnick *et al.* (2008) went in the direction expected under the deterministic theory—a significant departure from the null (one-tailed binomial $P = 0.048$). Given our results, we could dismiss the results of Bolnick *et al.* (2008) as a chance observation that fell slightly below nominal significance. Although our results are statistically inconsistent with theirs, the discrepancy is relatively slight. For instance, in Figure 3B, only 30 of 74 crosses support the deterministic theory. If we use a χ^2 test to compare that with 13 of 18 from Bolnick *et al.* (2008), we

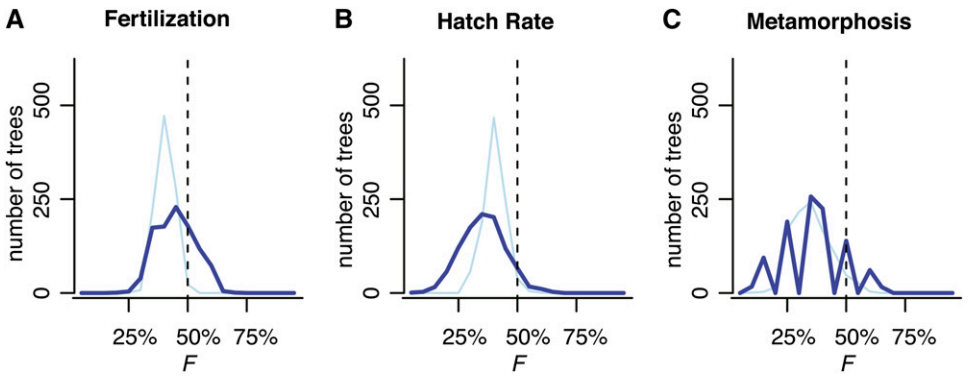

Figure 3 Asymmetries in mitochondrial *vs.* nuclear rates of evolution do not explain asymmetries in mating or hybrid viability. We examined asymmetries across a distribution of 1000 plausible phylogenetic trees (of varying topologies and branch lengths). Let *C* denote the most recent common ancestor of species A and B, and let $L(m)_{iC}$ ($L(n)_{iC}$) denote the estimated number of mitochondrial (nuclear) substitutions (branch length) separating species *C* and *i*. Following Bolnick *et al.* (2008, Equation 1 and Figure 1), we calculate the relative rate of mtDNA evolution for lineage A *vs.* lineage B as $\delta_A = [L(m)_{AC}/(L(m)_{AC} + L(m)_{BC})] - [L(n)_{AC}/(L(n)_{AC} + L(n)_{BC})]$. For each tree, we calculated *F*, the fraction of crosses in which the lineage with the elevated relative rate of mtDNA to nuclear evolution is the worse dam (*i.e.*, produces lower rates of fertilization, hatching, or metamorphosis). This corresponds to $\delta_A \rho < 0$. In each panel, the *x*-axis is *F* and the *y*-axis is the number of trees (from our posterior distribution of 1000) that produce each *F*. The *y*-axis accounts for phylogenetic uncertainty. Light blue lines include all data and dark blue lines are node-weighted averages (*i.e.*, the data after phylogenetic correction). If the deterministic theory was supported, we expect $F > 0.5$ for a significant majority of trees, at least for B and C, which report phenotypes likely to be affected by mitonuclear incompatibilities. (A) Lower fertilization occurs when the maternal lineage has an elevated relative rate of mtDNA evolution ($\delta_A > 0$) for only 43.4 of 107 crosses when averaged over our 1000 trees, *i.e.*, $F = 0.41$ (10.90 of 23.98 after phylogenetic correction, $P = 0.45$). After phylogenetic correction, only one-fifth of trees (200 of 1000) produce $F > 0.5$, and only 1 of our 1000 trees produces *F* significantly larger than 0.5. (B) For hatching, on average 29.68 of 74 crosses support the deterministic theory, $F = 0.40$ (7.10 of 20.00 after phylogenetic correction, $P = 0.36$). Only one-thirtieth of trees (33 of 1000) produce $F > 0.5$, and none of our 1000 trees produces *F* significantly larger than 0.5. (C) In metamorphosis, on average 7.97 of 22 crosses support the deterministic theory, $F = 0.36$ (4.32 of 12 after phylogenetic correction, $F = 0.36$). After phylogenetic correction, only one-thirteenth (33 of 1000) of trees produce $F > 0.5$, and none of our thousand trees does so significantly.

reject homogeneity with $P = 0.03$. Yet, each data set is consistent with a very small positive signal associated with mitonuclear DMIs. (For instance, if the binomial probability (p) that the dam with $\delta_A > 0$ produces the less fit F_1 is raised to 0.507 instead of 0.5, the probability of seeing as many "concordant" results as Bolnick *et al.* (2008) becomes $P > 0.05$. But seeing as few concordant results as we did also has $P > 0.05$.) Thus, both results could be somewhat unlikely outcomes of a subtle influence of relative mitochondrial-to-nuclear substitution rates on viability in reciprocal crosses. Our negative result cannot be simply attributed to misidentifying the sign of relative mitonuclear rates in cases with subtle differences—even the lineage with the highest relative rate of mitochondrial substitution does not produce particularly poor dams (see Table S3, Table S4, and File S1).

Our analyses can be refined in several ways. Analyses of complete nuclear and mitochondrial genomes could replace approximations of their relative rates of evolution. Alternatively, a clearer signal may be found by considering only nuclear and mitochondrial loci known to interact. Nevertheless, our molecular data are comparable to those of Bolnick *et al.* (2008), and we analyze many more crosses. Data from additional taxa would be welcome. Rapid advances in sequencing technology will simplify the molecular analyses, but experimental crosses will, unfortunately, remain laborious.

A notable finding of our analysis is a deep discordance between mitochondrial and nuclear topologies. This discordance and numerous other potential cases of mitochondrial introgression (Toews and Brelsford 2012) demonstrate that mitonuclear incompatibilities need not bar interspecific gene flow. In contrast, data mapping hybrid incompatibilities to mitochondria (Fishman and Willis 2006; Rieseberg and Blackman 2010) and physiological arguments (Rand *et al.* 2004; Gershoni *et al.* 2009; Chou and Leu 2010; Lane 2011; Burton and Barreto 2012) suggest that mitochondria can play a major role in reproductive isolation. These apparently contradictory results may simply reflect the stochasticity of substitutions and the heterogeneity of effects of mitochondrial introgressions into foreign genetic backgrounds. These effects can range from largely innocuous (or even favorable) to profoundly disruptive.

Acknowledgments

We thank Dan Bolnick, Daniel Matute, Leonie Moyle, and David Rand for their constructive comments. We also thank David Cannatella for permission to use previously unpublished RAG1 sequence data. For the loan of tissue samples or permission to use DNA extractions generated for prior research, we thank David Blackburn and Jens Vindum (California Academy of Sciences), Rafe Brown and Linda Trueb (University of Kansas Biodiversity Institute), Jonathan Campbell (University of Texas, Arlington Collection of Vertebrates), David Cannatella and Travis LaDuc (Texas Natural History Collections, University of Texas, Austin), Jim McGuire (Museum of Vertebrate Zoology, University of California, Berkeley), Alan Resetar (Field Museum of Natural History), and Addison Wynn (United States National Museum). This research was supported by grants from the National Science Foundation: DEB 0815145 to M.T., a National Science Foundation Bioinformatics postdoctoral fellowship to Y.B., and a predoctoral fellowship to M.R.M.; and by National Institutes of Health R01 GM104325 to M.T.

Literature Cited

Blair, W. F., 1972 *Evolution in the Genus* Bufo. University of Texas Press, Austin, TX.

Bolnick, D. I., M. Turelli, H. López-Fernández, P. C. Wainwright, and T. J. Near, 2008 Accelerated mitochondrial evolution and 'Darwin's corollary': asymmetric viability of reciprocal F_1 hybrids in centrarchid fishes. Genetics 178: 1037–1048.

Burton, R. S., and F. S. Barreto, 2012 A disproportionate role for mtDNA in Dobzhansky–Muller incompatibilities? Mol. Ecol. 21: 4942–4957.

Burton, R. S., C. K. Ellison, and J. S. Harrison, 2006 The sorry state of F_2 hybrids: consequences of rapid mitochondrial DNA evolution in allopatric populations. Am. Nat. 168: S14–S24.

Chou, J. Y., and L. Y. Leu, 2010 Speciation through cytonuclear incompatibility: insights from yeast and implications for higher eukaryotes. BioEssays 32: 401–411.

Chou, J. Y., Y. S. Hung, K. H. Lin, H. Y. Lee, and J. Y. Leu, 2010 Multiple molecular mechanisms cause reproductive isolation between three yeast species. PLoS Biol. 8: e1000432.

Darwin, C., 1859 *On the Origin of Species*. Murray, London.

Drummond, A. J., M. A. Suchard, D. Xie, and A. Rambaut, 2012 Bayesian phylogenetics with BEAUTi and the BEAST 1.7. Mol. Biol. Evol. 29: 1969–1973.

Ellison, C. K., and R. S. Burton, 2008 Interpopulation hybrid breakdown map to the mitochondrial genome. Evolution 62: 631–638.

Fishman, L., and J. H. Willis, 2006 A cytonuclear incompatibility causes anther sterility in *Mimulus* hybrids. Evolution 60: 1372–1381.

Fitzpatrick, B. M., 2002 Molecular correlates of reproductive isolation. Evolution 56: 191–198.

Gershoni, M., A. R. Templeton, and D. Mishmar, 2009 Mitochondrial bioenergetics as a major motive force of speciation. BioEssays 31: 642–650.

Lane, N., 2011 Mitonuclear match: optimizing fitness and fertility over generations drives ageing within generations. BioEssays 33: 860–869.

Lee, H. Y., J. Y. Chou, L. Cheong, N. H. Chang, S. Y. Yang *et al.*, 2008 Incompatibility of nuclear and mitochondrial genomes causes hybrid sterility between two yeast species. Cell 135: 1065–1073.

Malone, J. H., and B. E. Fontenot, 2008 Patterns of reproductive isolation in toads. PLoS ONE 3: e3900.

Meiklejohn, C. D., M. A. Holmbeck, M. A. Siddiq, D. N. Abt, D. M. Rand *et al.*, 2013 An incompatibility between a mitochondrial tRNA and its nuclear-encoded tRNA synthetase compromises development and fitness in *Drosophila*. PLoS Genet. 9: e1003238.

Montooth, K. L., C. D. Meiklejohn, D. N. Abt, and D. M. Rand, 2010 Mitochondrial-nuclear epistasis affects fitness within species but does not contribute to fixed incompatibilities between species of *Drosophila*. Evolution 64: 3364–3379.

Orr, H. A., 1993 A mathematical model of Haldane's rule. Evolution 47: 1606–1611.

Pauly, G. B., D. M. Hillis, and D. C. Cannatella, 2009 Taxonomic freedom and the role of official lists of species names. Herpetologica 65: 115–128.

R Development Core Team, 2008 R: a language and environment for statistical computing. R Foundation for Statistical Computing, Vienna, Austria. http://www.R-project.org.

Rand, D. M., R. A. Haney, and A. J. Fry, 2004 Cytonuclear cooperation: the genomics of cooperation. Trends Ecol. Evol. 19: 645–653.

Rieseberg, L. H., and B. K. Blackman, 2010 Speciation genes in plants. Ann. Bot. 106: 439–455.

Ronquist, F., M. Teslenko, P. van der Mark, D. Ayres, A. Darling *et al.*, 2012 MrBayes 3.2: efficient Bayesian phylogenetic inference and model choice across a large model space. Syst. Biol. 54: 401–418.

Toews, D. P. L., and A. Brelsford, 2012 The biogeography of mitochondrial and nuclear discordance in animals. Mol. Ecol. 21: 3907–3930.

Turelli, M., and L. C. Moyle, 2007 Asymmetric postmating isolation: Darwin's corollary to Haldane's rule. Genetics 176: 1059–1088.

Vacquier, V. D., and W. J. Swanson, 2011 Selection in the rapid evolution of gamete recognition proteins in marine invertebrates. Cold Spring Harb. Perspect. Biol. 3: a002931.

Wang, H., and S. K. Dey, 2006 Roadmap to embryo implantation: clues from mouse models. Nat. Rev. Genet. 7: 185–199.

Communicating editor: S. I. Wright

GENETICS

Supporting Information
http://www.genetics.org/lookup/suppl/doi:10.1534/genetics.113.161133/-/DC1

Explaining Darwin's Corollary to Haldane's Rule: The Role of Mitonuclear Interactions in Asymmetric Postzygotic Isolation Among Toads

Yaniv Brandvain, Gregory B. Pauly, Michael R. May, and Michael Turelli

DOI: 10.1534/genetics.113.161133

File S1

Supporting Material

1 Data

1.1 Sequence Data

The dataset included sequences for one mitochondrial region (12S, 16S, and the intervening $tRNA^{Val}$) and five nuclear genes: CXCR-4, Histone 3A, POMC, RAG1, and Rhodopsin (Table S1). Sequence data were gathered from available GenBank sequences with further sequencing to complete the dataset. When GenBank sequences were available from multiple conspecific individuals for the same gene, we selected the individual that was geographically and/or taxonomically (*i.e.*, same subspecies or closely related based on available phylogeographic data) closest to the source populations used in the original crossing experiments. Localities of source populations were determined from Blair (1972) and references therein. We used the same criterion for identifying the most appropriate tissue samples for those species for which additional sequencing was needed to fill out the data matrix.

Amplification conditions and primers follow Pauly *et al.* (2004) for the mtDNA region, Biju and Bossuyt (2003) for CXCR-4 (primers CXCR-4C and CXCR-4F), Colgan *et al.* (1999) for Histone 3A (primers H3F and H3R), Wiens *et al.* (2005) for POMC (primers POMC1 and POMC2), and Pauly (2008) for Rhodopsin. These Rhodopsin primers amplify an approximately 755bp region of Rhodopsin that overlaps a shorter fragment commonly used in anuran phylogenetic studies. The primers for RAG1 are provided in Table S2.

Alignments (see File S2) were generated using MUSCLE in Geneious Pro 5.1.6 (Biomatters Ltd.). The final aligned datasets resulted in 2491bp of mtDNA, 708bp of CXCR-4, 328bp of Histone 3A, 549bp of POMC, 2883bp of RAG1, and 309bp of Rhodopsin. All datasets were complete except that only partial sequences were obtained for three individuals for RAG1. Similar to Pauly *et al.* (2004), seven regions of the mtDNA alignment were excluded from analysis because they were difficult to align (106bp excluded yielding 2385bp for analysis); all seven regions correspond to loops in the secondary structure of 12S or 16S.

1.2 Taxon Sampling

Taxon sampling included 36 species (Table S1). *Bufo (Rhaebo) haematiticus* was specified as the outgroup. All recent studies of bufonids have identified our ingroup as monophyletic with respect to *B. haematiticus* (Pauly *et al.* 2004; Frost *et al.* 2006; Pramuk *et al.* 2008; Van Bocxlaer *et al.* 2010; Pyron and Wiens 2011). The 35 ingroup species were selected because crossing data were available and either existing sequences or tissue samples could be obtained to construct a multilocus dataset.

2 Tree Inference

2.1 MrBayes Analyses

For each of the following analyses, Bayesian phylogenetic inference was performed using MrBayes 3.2 (Ronquist *et al.* 2012). Each MCMC was run with two independent chains, each with four incrementally heated subchains. Each sampler was run for 20 million generations. Convergence for all parameters was then assessed using Tracer 1.5 for continuous parameters (Rambaut and Drummond 2009) and the slide command in AWTY for tree topology (Nylander *et al.* 2008). Samples drawn before all parameters converged, or the first 25% of the samples (if greater than the convergence time), were discarded as burn-in. For each MCMC, we performed a paired analysis under the prior (`mcmc data=no` in MrBayes) and compared the marginal distributions of continuous parameters between the prior and the posterior in Tracer 1.5. Because Bayesian phylogenetic inference tends to be robust to overparameterization (Huelsenbeck and Rannala 2004), we assumed that each data partition was evolving according to the

GTR+Γ substitution model, but considered simpler models if the more parameter-rich model proved to be pathological.

We flagged any particular analysis as pathological if it met any of the following criteria: 1) any parameter (including the tree topology) failed to converge in 20 million generations; 2) independent samplers failed to converge to the same marginal posterior distribution for any parameter (including the tree topology); 3) the effective sample size for any parameter was low (< 200); 4) the joint marginal posterior distribution for any pair of model parameters (particularly for exchangeability parameters within data partitions) was strongly ridged, indicating parameter interaction; 5) the marginal prior distributions were not different from the marginal posterior distributions, as determined by comparing the MCMC with and without data. When an analysis was determined to be pathological, we simplified the substitution model (*e.g.*, from GTR+Γ to HKY+Γ).

2.1.1 Gene Tree Analyses

We estimated separate gene trees for each locus using the protocol described above. Several loci had pathological substitution model parameters under the GTR+Γ model. In these cases, the HKY+Γ substitution models did not suffer from the same pathologies. For each locus, we identified the most parameter-rich model that did not suffer from MCMC pathologies for use in downstream analyses. We identified the GTR+Γ model for Rag1, CXCR4, and the mitochondrial sequence data, and the HKY+Γ model for Rhodopsin, POMC, and Histone3.

Across gene trees, clade posterior probabilities were quite low, likely due to the relatively small amount of data in individual loci. See Figures S1 to S6 for the Bayesian consensus trees resulting from the gene tree analyses.

2.1.2 Mitochondrial Introgression

Preliminary analyses indicated the presence of a mitochondrial introgression event in our phylogeny (G.B. Pauly and D. C. Cannatella, unpubl.), which would result in discordance between a shared nuclear tree and a mitochondrial tree. We estimated a tree for the combined (but partitioned) nuclear loci using the substitution models identified above for each partition. We also estimated a tree for the mitochondrial loci, and a tree for the combined (partitioned) nuclear and mitochondrial loci. Clade posterior probabilities for nuclear and mitochondrial trees were higher than for the individual gene tree analyses, but many clades were still weakly supported (Figure S7). For the combined analysis, clade posterior probabilities were very high (Figures S8 and S9).

We note that high clade posterior probabilities may reflect inflated confidence due to an underparameterized model – if there are two underlying tree topologies (one mitochondrial, the other nuclear), then the combined analysis does not have enough parameters to fully describe the data, and thus our estimate of the tree topology will be biased. Additionally, we repeated our downstream asymmetry analysis excluding all crosses spanning the mitochondrial introgression event; results were qualitatively the same, suggesting that our results are robust to the mitochondrial introgression (data not shown).

Both mitochondrial and nuclear analyses recovered four main clades consistent with broad biogeographic regions and previous analyses of bufonids (Pauly *et al.* 2004; Pramuk *et al.* 2008; Van Bocxlaer *et al.* 2010; Pyron and Wiens 2011). These clades include the Nearctic *Anaxyrus*, the Middle American *Incilius*, the South American *Rhinella*, and a fourth Old World clade that includes the African *Amietophrynus* and the Asian *Duttaphrynus* (we use these names as unranked clade names within the genus *Bufo*). This fourth clade includes the Eurasian species *Bufo viridis* in the nuclear results, but its placement is less clear in the mitochondrial results.

Comparing the mitochondrial, nuclear, and combined analyses reveals evidence for a deep mitochondrial introgression event (Figure S10). It is clear that the greatest disagreement among the tree topologies is the location of *Rhinella*. In the nuclear tree, *Rhinella* is most closely related to the Old World clade, while in the mitochondrial tree it is most closely related to *Anaxyrus*. In the combined analysis, *Rhinella* is sister to *Anaxyrus* + *Incilius*. We believe this supports the following scenario: early in the evolution of this group, a common ancestor of *Rhinella* inherited mitochondria from a common ancestor of *Anaxyrus*. This introgression event has resulted in a close sister relationship between *Rhinella* and *Anaxyrus* in the mitochondrial tree, and an "averaging" of nuclear and mitochondrial evidence in the combined tree (*i.e.*, *Rhinella* is being pulled towards the Old World clade by nuclear information and towards *Anaxyrus* by mitochondrial information).

2.1.3 Constrained Analysis

Deep discordance between nuclear and mitochondrial loci has the potential to introduce error in measurements of substitution rate asymmetry. In order to accommodate the deep discordance event, we estimated a tree for combined nuclear and mitochondrial data (partitioned by locus) using the previously identified substitution models, but enforced the deep relationships present in the nuclear tree. This allowed us to estimate branch lengths on a shared tree topology, and leverage information from mitochondrial and nuclear data to resolve more recent relationships. Additionally, we unlinked branch length parameters between mitochondrial and nuclear partitions in order to estimate these parameters separately, which was necessary to calculate asymmetrical rates of mitochondrial and nuclear substitution for later analyses. Clade posterior probabilities were high for all nodes (Figures S11 and S12). The sample of tree topologies was dominated by a single tree with marginal posterior probability 0.934; the next-best tree had a marginal posterior probability of 0.041.

2.2 BEAST Analysis

To understand the evolutionary tempo of reproductive isolation, we estimated an ultrametric tree using BEAST 1.7.4 (Drummond *et al.* 2012). We used the same substitution models and topological constraints as in the constrained analysis in MrBayes above. We used separate uncorrelated log-normal relaxed molecular clocks for nuclear and mitochondrial partitions. The consensus tree estimated by BEAST (Figure S13) is topologically identical to the rooted consensus tree estimated by MrBayes for the constrained analysis.

3 Posterior Samples for Asymmetry Analyses

Our asymmetry analyses depend critically on branch lengths as well as tree topology; despite a high degree of support for tree topology, we might be misled if we fail to account for uncertainty in branch lengths. To account for branch length and (minor) topological uncertainty, we drew 1000 samples from the post-burnin MCMCs for the constrained analysis described above (section S2.1.3, 500 samples from each of the paired runs). For each sampled generation, we drew the tree topology shared between nuclear and mitochondrial loci, along with its corresponding nuclear and mitochondrial branch lengths; these samples constitute a numerical approximation of the joint posterior distribution of tree topology, nuclear branch lengths, and mitochondrial branch lengths. Repeating our asymmetry analysis on each tree in this sample effectively averages over tree topology and branch lengths in proportion to their posterior probability.

4 Crosses to the clade with the largest relative rate of mitochondrial evolution do not support the deterministic theory

To focus on data most likely to reveal a deterministic mitonuclear signal, we looked separately at crosses that span the branch in Figure 1 with the greatest ratio of mitochondrial to nuclear substitutions, namely crosses involving *B. maculatus* or *B. regularis*. For hatching, a minority of crosses to both *B. maculatus* and *B. regularis* support the deterministic theory. There are only two observations involving metamorphosis, and both went in the expected direction. Combining the hatching and metamorphosis data from this select sample (without phylogenetic correction), fewer than half go in the expected direction.

References

Biju, S. D. and Bossuyt, F. (2003) New frog family from India reveals an ancient biogeographical link with the Seychelles. Nature **425 :** 711–714.

Blair, W. F. (1972) *Evolution in the Genus* Bufo. Austin, TX: University of Texas Press.

Colgan, D. J., McLauchlan, A., Wilson, G. . D. F., Livingston, S. P., Edgecombe, G. D., Macaranas, J., Cassis, G., and Grey, M. R. (1999) Histone H3 and U2 snRNA DNA sequences and arthropod molecular evolution. Australian Journal of Zoology **46 :** 419–437.

Drummond, A. J., Suchard, M. A., Xie, D., and Rambaut, A. (2012) Bayesian phylogenetics with BEAUti and the BEAST 1.7. Molecular Biology and Evolution **29 :** 1969–1973.

Frost, D. R., Grant, T., Faivovich, J., Bain, R. H., Haas, A., Haddad, C. F. B., Sa, R. R. D., Channing, A., Wilkinson, M., Donnellan, S. C., Raxworthy, C. J., Campbell, J. A., Blotto, B. L., Moler, P., Drewes, R. C., Nussbaum, R. A., Lynch, J. D., Green, D. M., and Wheeler, W. C. (2006) The amphibian tree of life. Bulletin of the American Museum of Natural History **297**.

Huelsenbeck, J. P. and Rannala, B. (2004) Frequentist properties of Bayesian posterior probabilities of phylogenetic trees under simple and complex substitution models. Systematic Biology **53 :** 904–913.

Nylander, J., Wilgenbusch, J., Warren, D., and Swofford, D. (2008) AWTY (are we there yet?): a system for graphical exploration of MCMC convergence in Bayesian phylogenetics. Bioinformatics **24 :** 581–583.

Pauly, G. B. (2008) "Phylogenetic systematics, historical biogeography, and the evolution of vocalizations in the Nearctic toads (*Bufo*)". PhD dissertation. University of Texas, Austin.

Pauly, G. B., Hillis, D. M., and Cannatella, D. C. (2004) The history of a nearctic colonization: molecular phylogenetics and biogeography of the Nearctic toads (*Bufo*). Evolution **58 :** 2517–2535.

Pramuk, J. B., Robertson, T., Sites, J. W., and Noonan, B. P. (2008) Around the world in 10 million years: biogeography of the nearly cosmopolitan true toads (Anura: Bufonidae). Global Ecology and Biogeography **17 :** 72–83.

Pyron, R. A. and Wiens, J. J. (2011) A large-scale phylogeny of Amphibia including over 2800 species, and a revised classification of extant frogs, salamanders, and caecilians. Molecular Phylogenetics and Evolution **61 :** 543–583.

Rambaut, A. and Drummond, A. J. (2009) *Tracer v1.5*. Available from: http://beast.bio.ed.ac.uk/Tracer. Edinburgh (United Kingdom): Institute of Evolutionary Biology, University of Edinburgh.

Ronquist, F., Teslenko, M., Mark, P. van der, Ayres, D. L., Darling, A., Höhna, S., Larget, B., Liu, L., Suchard, M. A., and Huelsenbeck, J. P. (2012) MrBayes 3.2: Efficient Bayesian phylogenetic inference and model choice across a large model space. Systematic Biology **61 :** 539–542.

Van Bocxlaer, I., Loader, S. P., Roelants, K., Biju, S. D., Menegon, M., and Bossuyt, F. (2010) Gradual adaptation toward a range-expansion phenotype initiated the global radiation of toads. Science **327 :** 679–682.

Wiens, J. J., Fetzner, J. W., Parkinson, C. L., and Reeder, T. W. (2005) Hylid Frog Phylogeny and Sampling Strategies for Speciose Clades. Systematic Biology **54 :** 778–807.

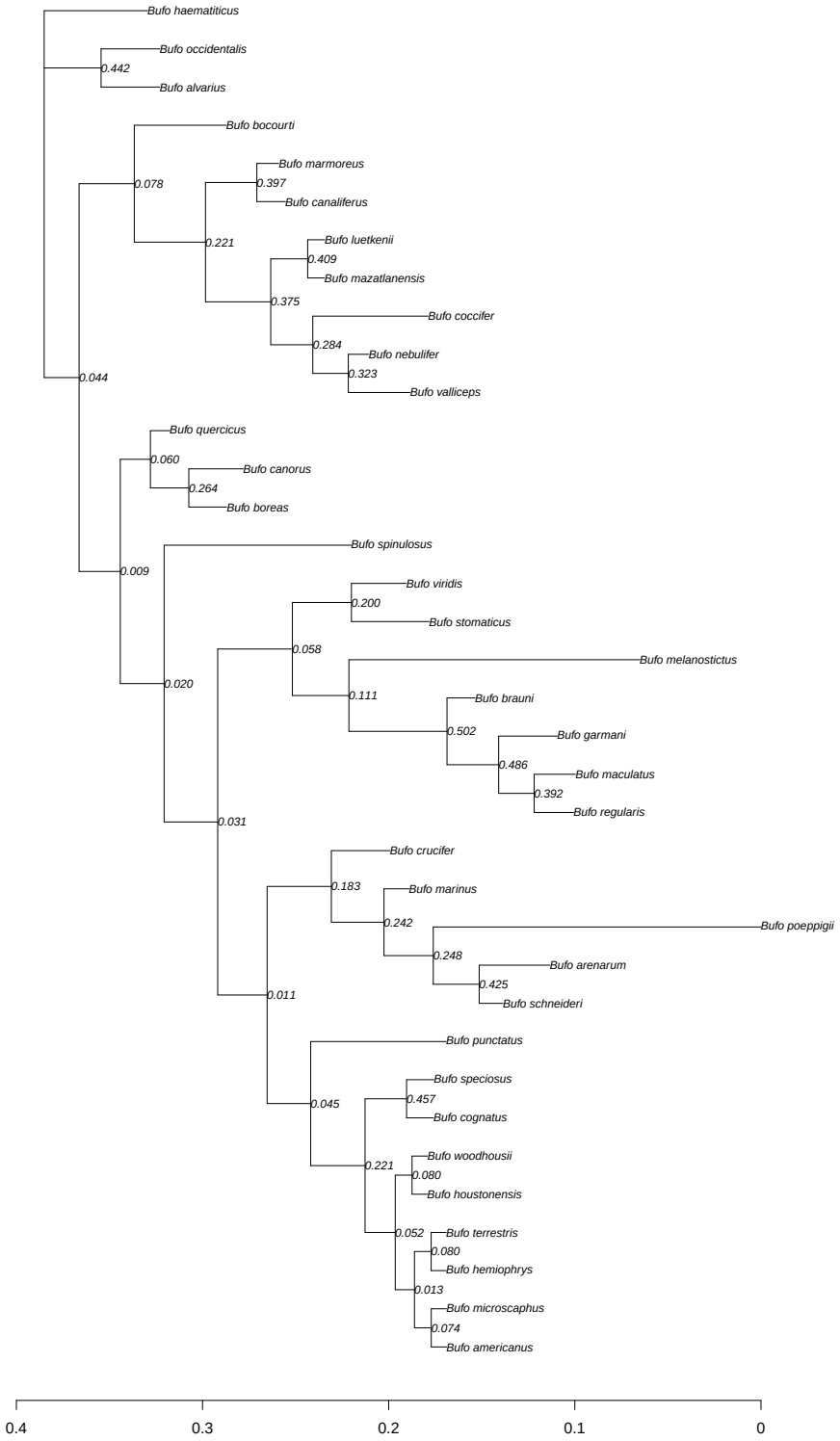

Figure S1: Consensus tree (using Contype = allcompat in MrBayes, which computes the 50% majority rule consensus tree and adds all groups compatible with that consesus tree, resulting in a final consensus tree which can have nodes with $< 50\%$ posterior probability) for Rhodopsin under the HKY+Γ model. Numbers on nodes are posterior probabilities. The scale bar is in expected number of substitutions.

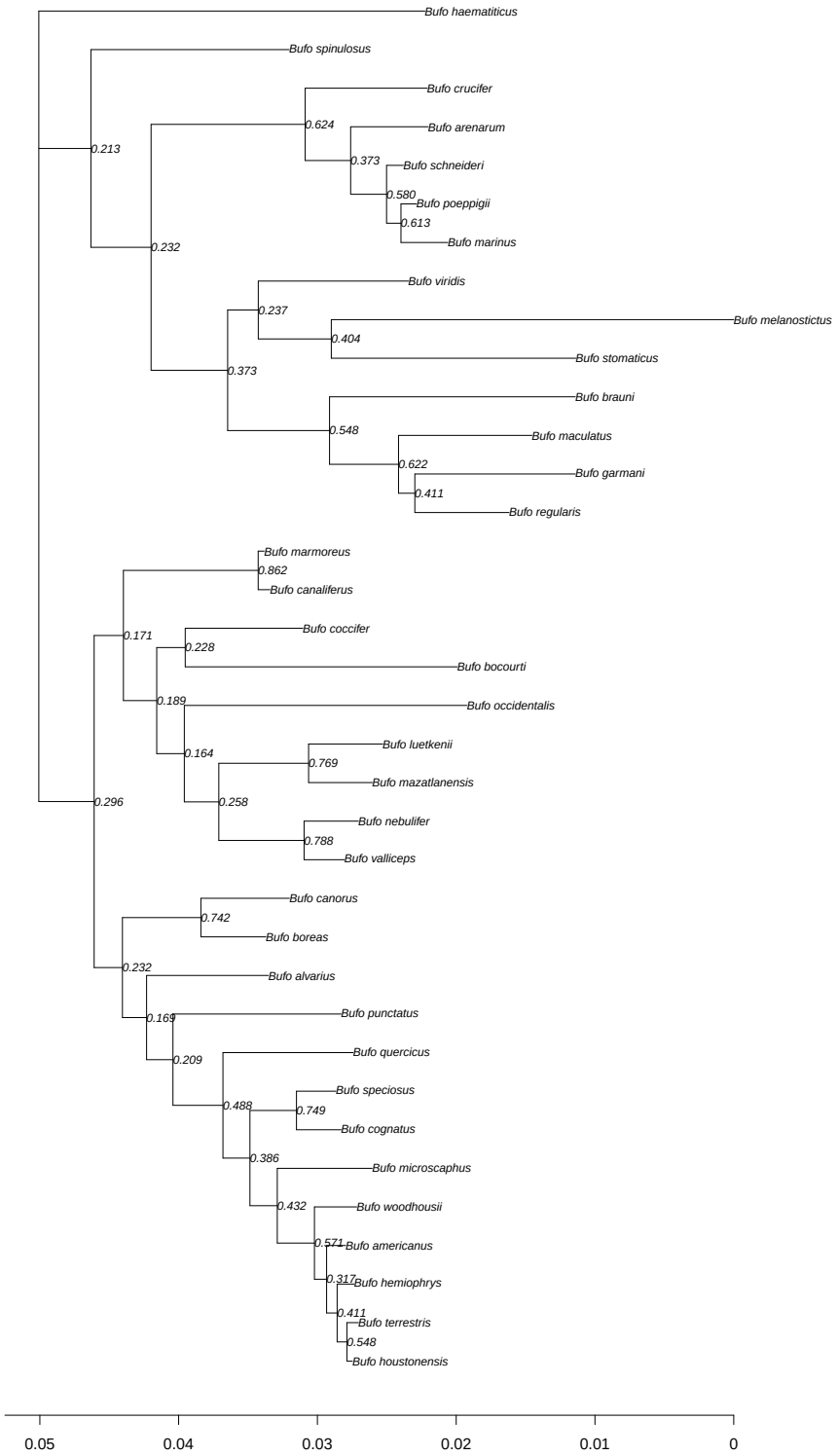

Figure S2: Consensus tree (see Figure S1) for Rag1 under the GTR+Γ model. Numbers on nodes are posterior probabilities. The scale bar is in expected number of substitutions.

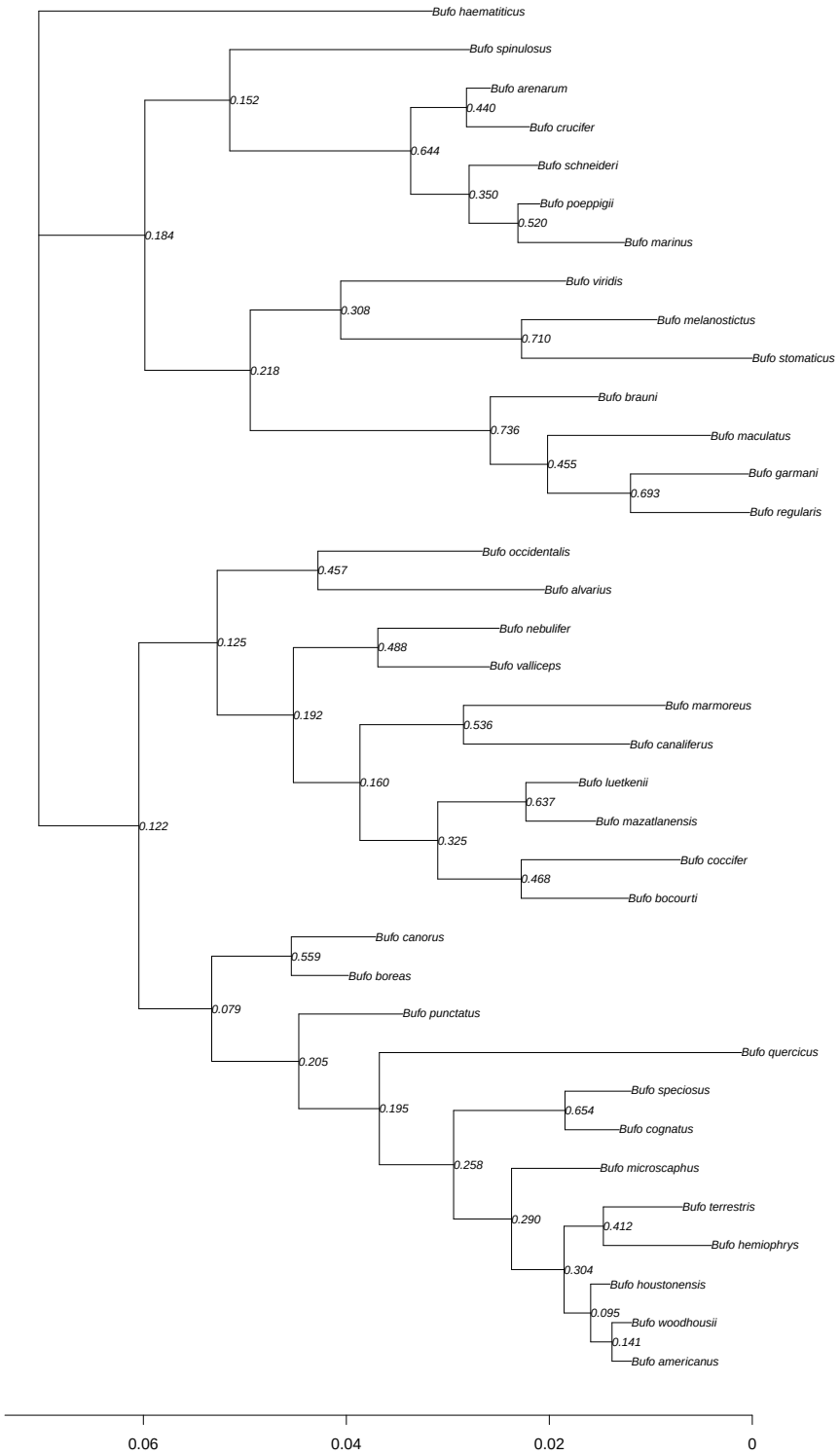

Figure S3: Consensus tree (see Figure S1) for CXCR4 under the GTR+Γ model. Numbers on nodes are posterior probabilities. The scale bar is in expected number of substitutions.

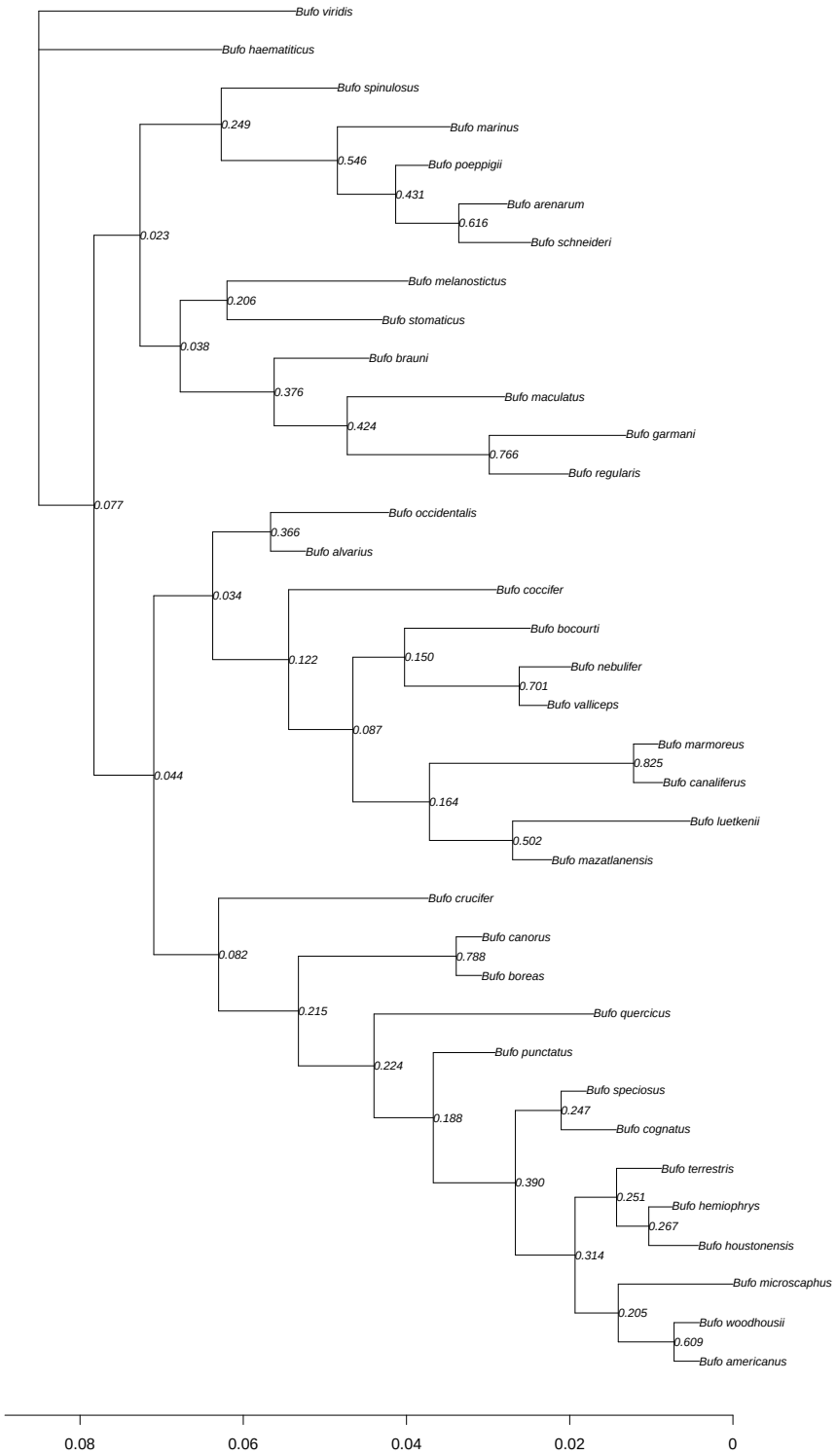

Figure S4: Consensus tree (see Figure S1) for POMC under the GTR+Γ model. Numbers on nodes are posterior probabilities. The scale bar is in expected number of substitutions.

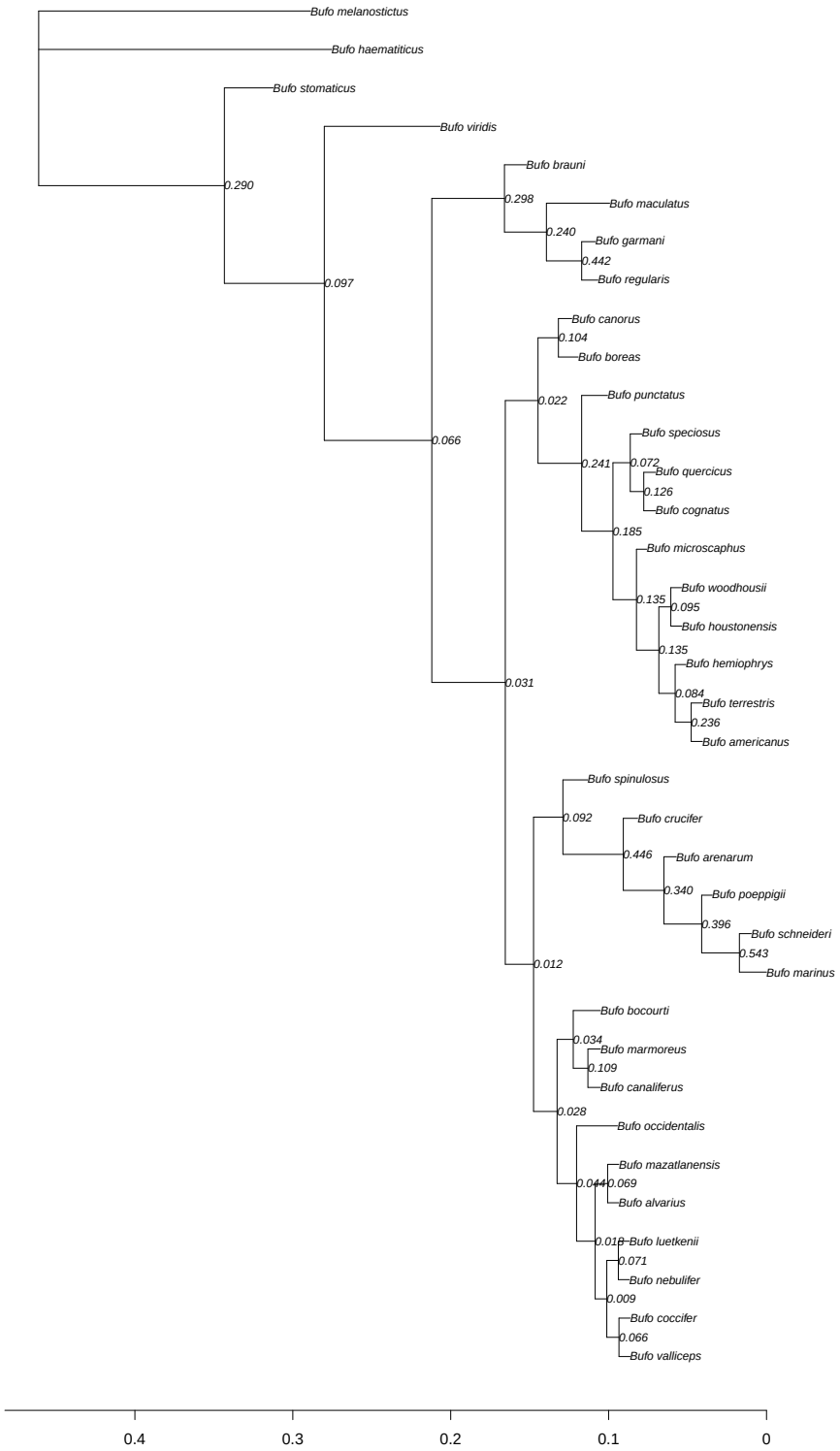

Figure S5: Consensus tree (see Figure S1) for Histone3 under the HKY+Γ model. Numbers on nodes are posterior probabilities. The scale bar is in expected number of substitutions.

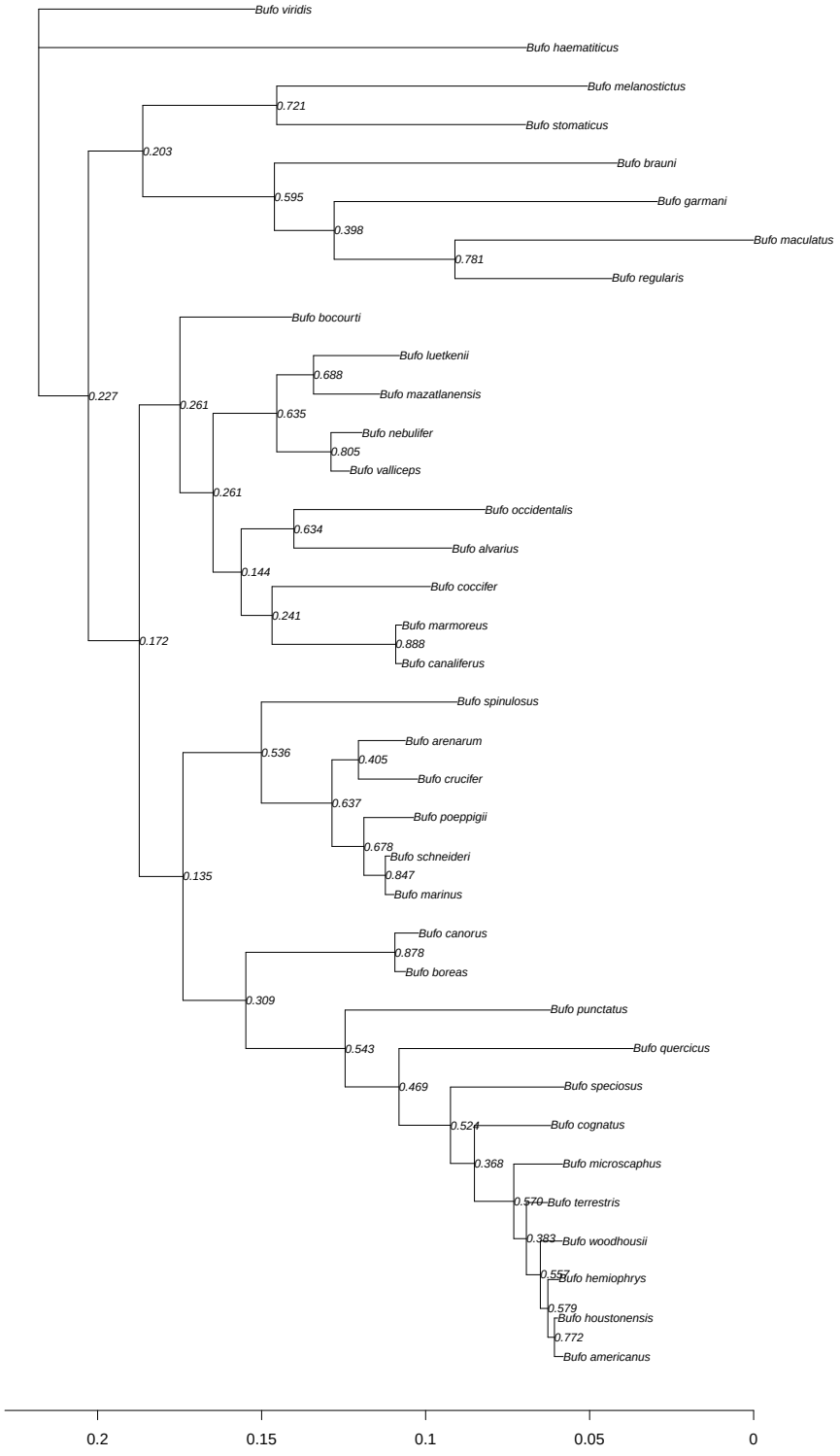

Figure S6: Consensus tree (see Figure S1) for mitochondrial data under the GTR+Γ model. Numbers on nodes are posterior probabilities. The scale bar is in expected number of substitutions.

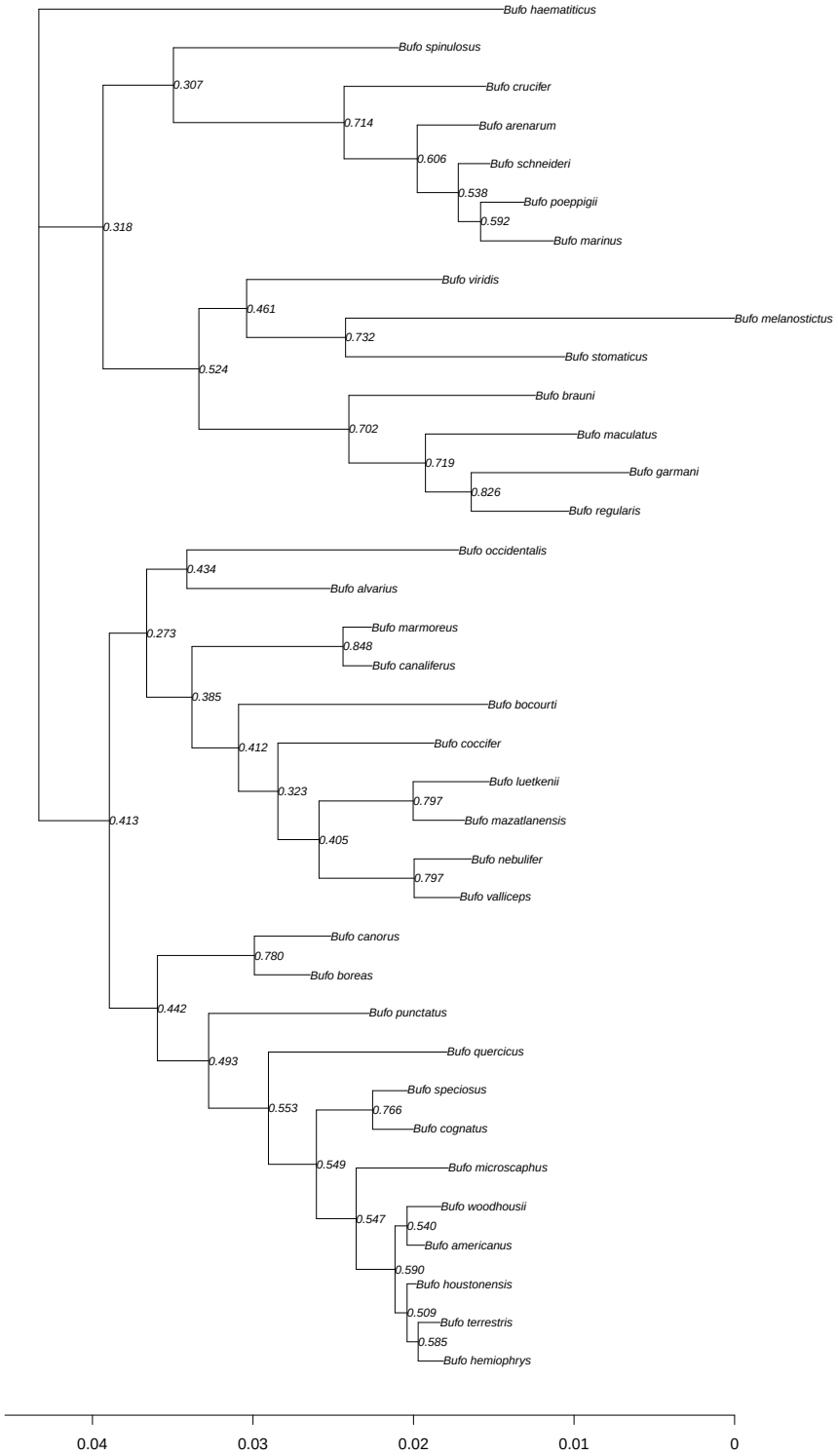

Figure S7: Consensus tree (see Figure S1) for nuclear data under a partitioned model. Numbers on nodes are posterior probabilities. The scale bar is in expected number of substitutions.

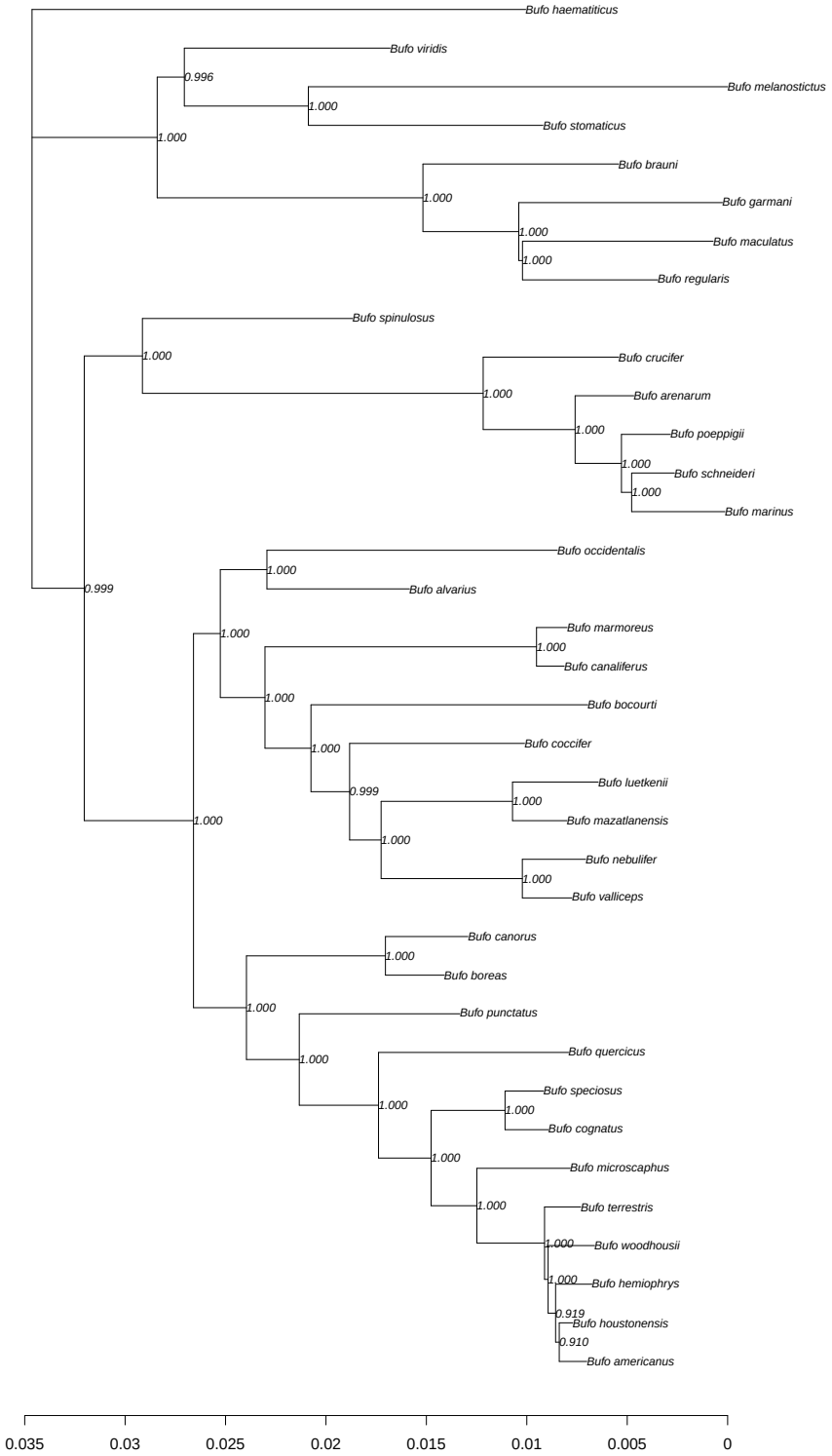

Figure S8: Consensus tree (see Figure S1) for combined data (nuclear and mitochondrial) partitioned by locus, with branch lengths for the nuclear loci. Numbers on nodes are posterior probabilities. The scale bar is in expected number of substitutions.

Figure S9: Consensus tree (see Figure S1) for combined data (nuclear and mitochondrial) partitioned by locus, with branch lengths for the mitochondrial loci. Numbers on nodes are posterior probabilities. The scale bar is in expected number of substitutions.

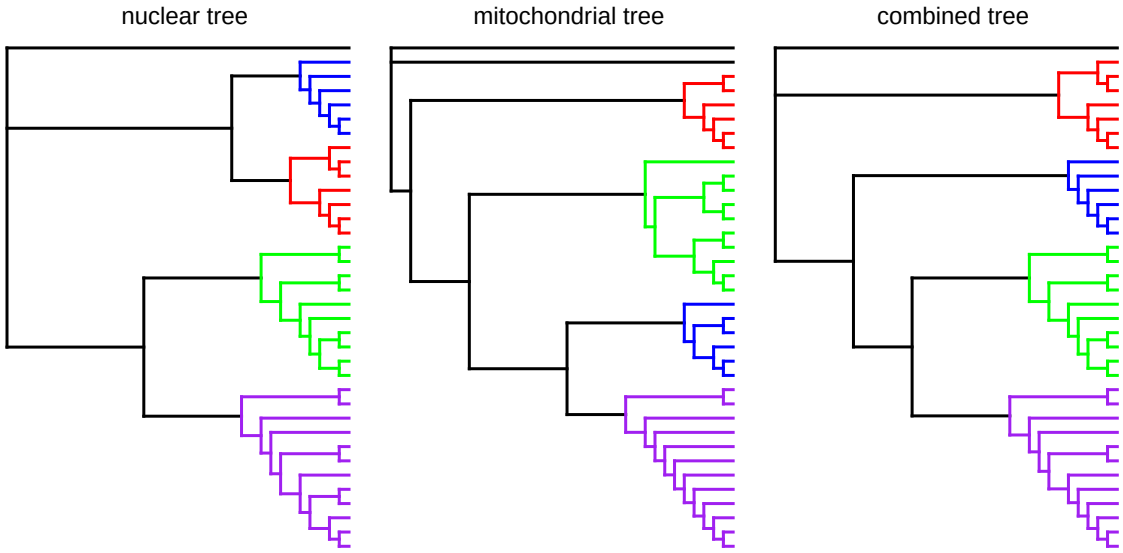

Figure S10: Comparison of trees from nuclear (left), mitochondrial (center), and combined (right) analyses. Names have been removed, and clades that are common across the topologies have been colored in order to highlight the mitochondrial introgression event as follows: the Nearctic *Anaxyrus* is in purple; the Middle American *Incilius* is in green; the South American *Rhinella* is in blue; and an Old World clade including African and Eurasian lineages is in red. In the nuclear tree, *Rhinella* (blue) is most closely related to the Old World clade (red). In the mitochondrial tree, *Rhinella* (blue) is most closely related to *Anaxyrus* (purple). In the combined tree, *Rhinella* (blue) is sister to the *Anaxyrus* + *Incilius*.

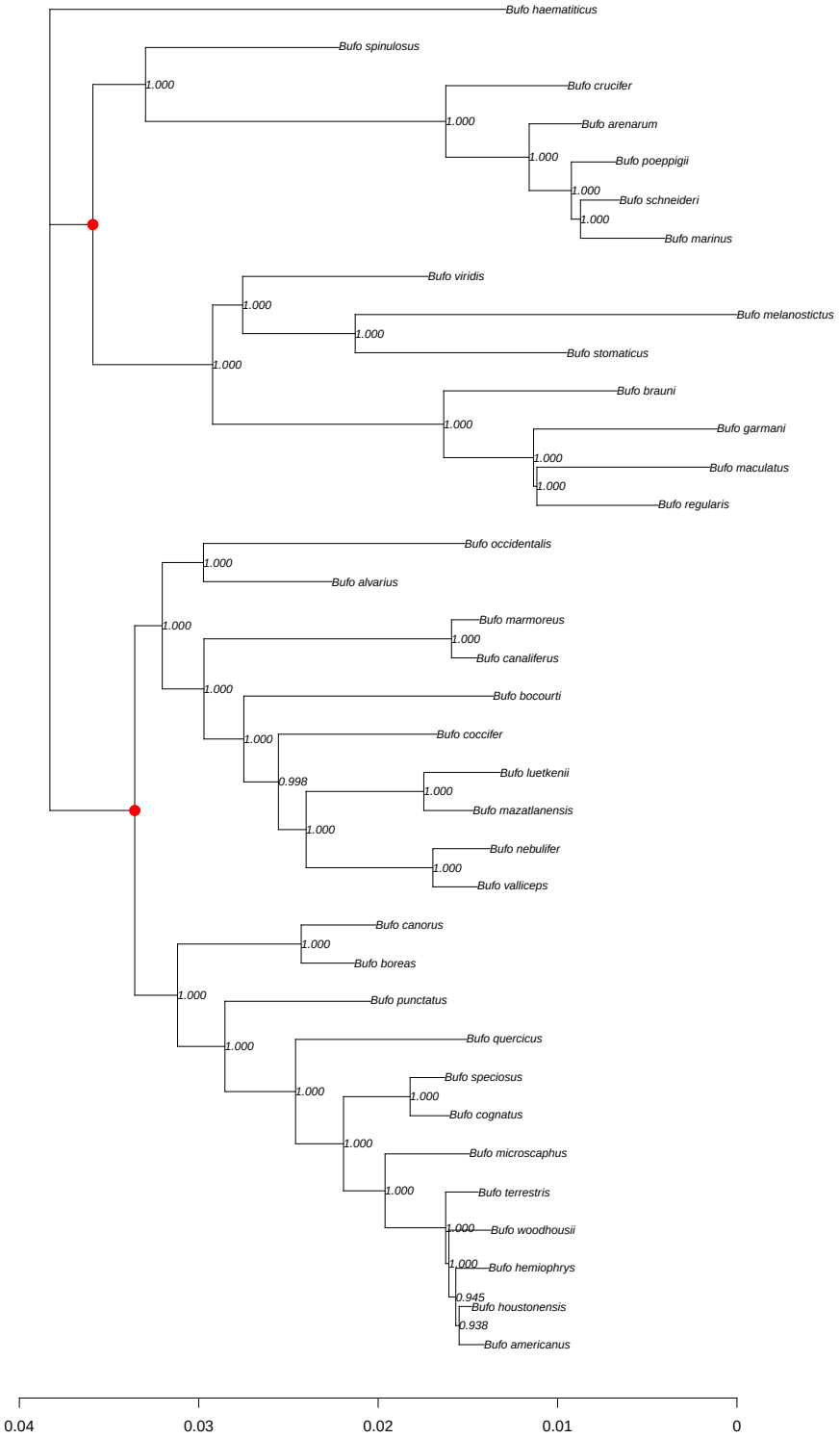

Figure S11: Consensus tree (see Figure S1) from constrained analysis for combined data (nuclear and mitochondrial) partitioned by locus, with branch lengths for the nuclear loci. Numbers on nodes are posterior probabilities. The scale bar is in expected number of substitutions. Red points indicate the constrained nodes.

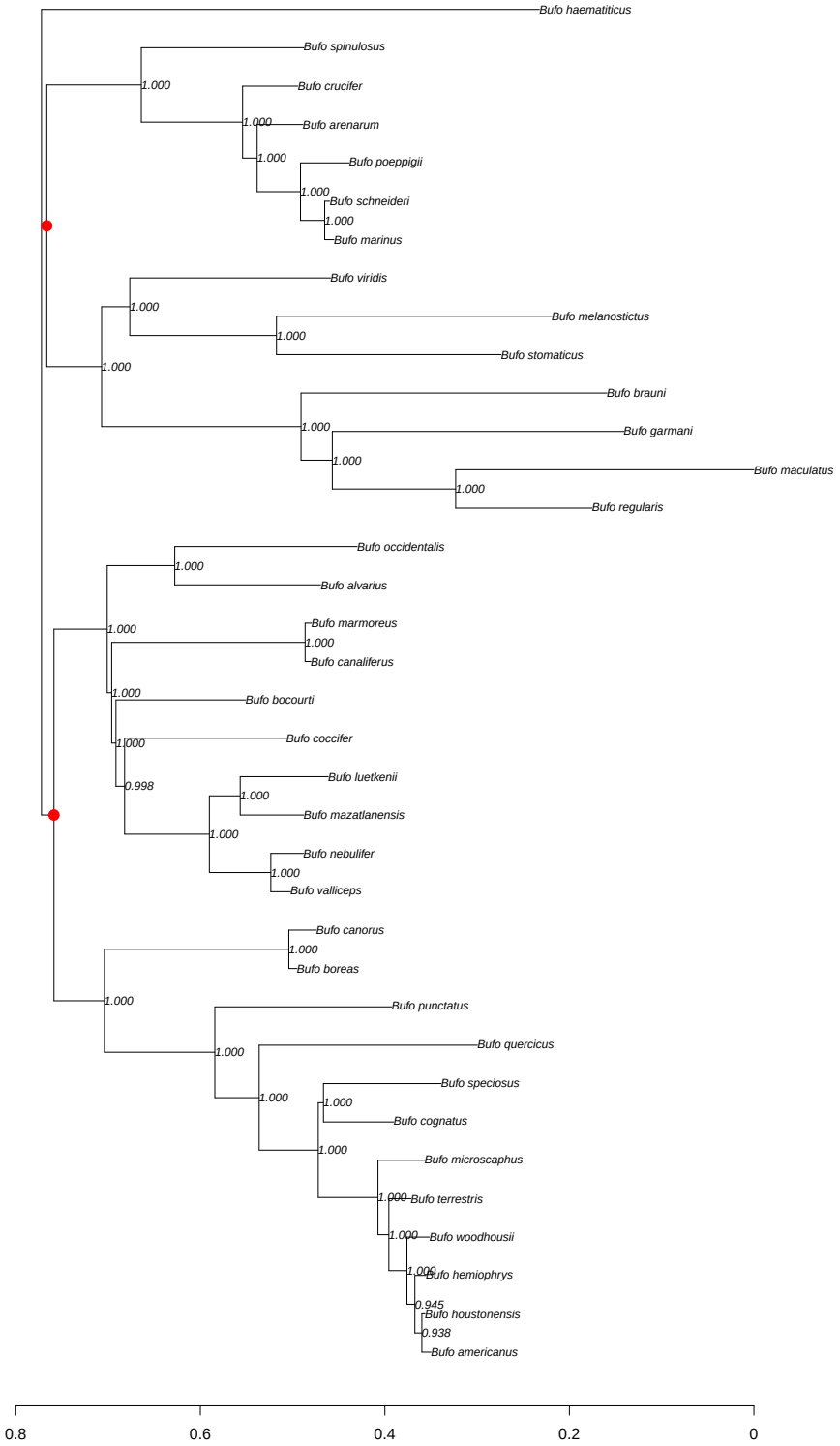

Figure S12: Consensus tree (see Figure S1) from constrained analysis for combined data (nuclear and mitochondrial) partitioned by locus, with branch lengths for the mitochondrial loci. Numbers on nodes are posterior probabilities. The scale bar is in expected number of substitutions.

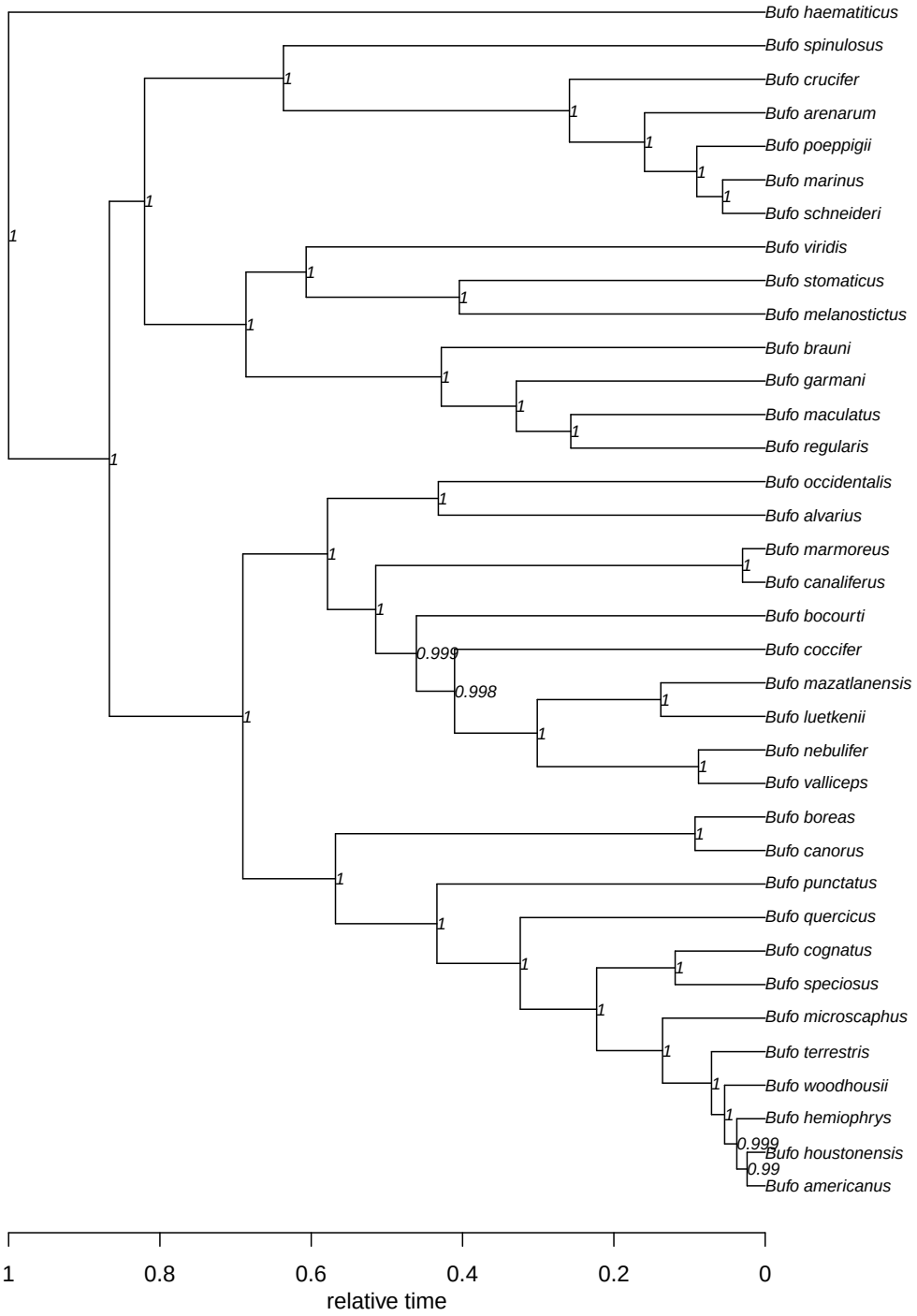

Figure S13: 50% Majority rule consensus tree from the BEAST analysis. Numbers on nodes are posterior probabilities. The scale bar is in relative time (with a tree height of 1).

species	mtDNA ID	mtDNA GB	CXCR4 ID	CXCR4 GB
B. americanus	TNHC (DMH88-79)	AY680205	not given	FJ882730
B. houstonensis	TNHC (DMH88-3)	AY680208	TNHC (DMH88-3)	KJ532317
B. hemiophrys	MVZ 137738	AY680213	MVZ 137738	KJ532318
B. woodhousii	TNHC 60511	AY680217	KU 224658	DQ306551
B. terrestris	MVZ 223379	AY680220	LSUMZ H2904	DQ306537
B. microscaphus	MVZ 223365	AY680227	USNM 320147	DQ306563
B. cognatus	MVZ 143048	AY680230	LSUMZ H457	DQ306502
B. speciosus	TNHC 60379	AY680229	TNHC (AHP3496)	KJ532319
B. quercicus	MVZ 223370	AY680235	LSUMZ H2921	DQ306549
B. punctatus	TNHC 58788	AY680236	TNHC 58788	KJ532320
B. boreas	MVZ 142827	AY680242	MVZ 223292	DQ306499
B. canorus	MVZ 142992	AY680239	MVZ 142992	KJ532321
B. bocourti	MVZ 143367	AY680245	UTA 50920	HM563894
B. alvarius	TNHC 61247	AY325984	USNM 320001	DQ306516
B. occidentalis	UTA 34111	AY680257	UTA 13543	HM563918
B. valliceps	UTA 13097	AY680253	MZFC (JRM3868)	HM563927
B. nebulifer	UTA 13119	AY680252	UTA 52489	HM563916
B. mazatlanensis	MVZ 132973	AY680254	MVZ 132967	HM563914
B. luetkenii	KU 289850	DQ158467	KU 289850	DQ306565
B. coccifer	KU 290030	DQ158443*	KU 290030	DQ306526
B. canaliferus	UTA 34110	AY680251	UTA 47640	HM563899
B. marmoreus	UTA 13032	AY680250	UTA 13032	HM563913
B. marinus	KU 205236	AY325994	KU 217482	DQ306544
B. schneideri	BB 1224	DQ283065	KU 289057	DQ306528
B. poeppigii	USNM 268824	DQ158481	USNM 268824	DQ306517
B. crucifer	ZUEC (DCC3392)	AY680260	ZUEC (DCC3392)	KJ532322
B. arenarum	AR305	DQ158429	AR305	DQ306529
B. spinulosus	NB96-23	AY680263	IdlR3837	DQ306566
B. regularis	KU 290435	DQ158485	KU 290435	DQ306523
B. maculatus	KU 290430	DQ158469	KU 290430	DQ306533
B. garmani	CAS 214829	DQ158453	CAS 214829	DQ306547
B. brauni	RdS 952	DQ283416	FMNH 251853	DQ306514
B. stomaticus	CAS 232071	KJ532264	not given	FJ882681
B. melanostictus	TNHC 59161	AY680268	TNHC (RMB1793)	KJ532323
B. viridis	TNHC 56752	AY680267	not given	FJ882714
B. haematiticus	MVZ 223359	AY680270	QCAZ 13215	DQ306501

Table S1: Sample and sequence information for all loci used in this analysis.
* Bases 1 - 110 from HM563828 (TCWC83998).
Part 1 of 3, continues on next page.

species	H3 ID	H3 GB	POMC ID	POMC GB
B. americanus	TNHC (DMH88-79)	KJ532296	KU 289469	DQ158268
B. houstonensis	TNHC (DMH88-3)	KJ532297	TNHC (DMH88-3)	KJ532281
B. hemiophrys	MVZ 137738	KJ532298	MVZ 137738	KJ532282
B. woodhousii	RNF 2417	DQ284222	KU 224658	DQ158339
B. terrestris	AMNH 168433	DQ284196	LSUMZ H2904	DQ158330
B. microscaphus	MVZ 223365	KJ532299	USNM 320147	DQ158318
B. cognatus	AMNH 168396	DQ284197	LSUMZ H457	DQ158285
B. speciosus	TNHC (AHP3496)	KJ532300	TNHC (AHP3496)	KJ532283
B. quercicus	MVZ 223370	KJ532301	LSUMZ H2921	DQ158325
B. punctatus	AMNH 168398	DQ284198	TNHC 58788	KJ532284
B. boreas	RNF 2416	DQ284215	MVZ 223292	DQ158278
B. canorus	MVZ 142992	KJ532302	MVZ 142992	KJ532285
B. bocourti	MVZ 143367	KJ532303	MVZ 143367	KJ532286
B. alvarius	ATH 499	DQ284289	USNM 320001	DQ158267
B. occidentalis	UTA 34111	KJ532304	UTA 34111	KJ532287
B. valliceps	UTA 13097	KJ532305	MZFC (JRM-3870)	DQ158333
B. nebulifer	UTA 13119	KJ532306	UTA 13119	KJ532288
B. mazatlanensis	MVZ 132973	KJ532307	MVZ 132973	KJ532289
B. luetkenii	MVZ 207144	KJ532308	KU 289850	DQ158308
B. coccifer	KU 290030	KJ532309	KU 290030	DQ158284
B. canaliferus	UTA 34110	KJ532310	UTA 34110	KJ532290
B. marmoreus	UTA 13032	KJ532311	UTA 13032	KJ532291
B. marinus	MJH 3678	DQ284092	KU 217482	DQ158316
B. schneideri	BB 1224	DQ284102	KU 289057	DQ158322
B. poeppigii	USNM 268824	KJ532312	USNM 268824	KJ532292
B. crucifer	ZUEC (DCC3392)	KJ532313	ZUEC (DCC3392)	KJ532293
B. arenarum	MACN 38639	DQ284103	AR305	DQ158271
B. spinulosus	BB 1032	DQ284077	IdlR3837	DQ158328
B. regularis	FMNH 251386	DQ284201	KU 290435	DQ158326
B. maculatus	AMNH 163573	DQ284374	KU 290430	DQ158310
B. garmani	CAS 214829	KJ532314	CAS 214829	DQ158294
B. brauni	FMNH 251853	KJ532315	FMNH 251853	DQ158279
B. stomaticus	CAS 232071	KJ532316	CAS 232071	KJ532294
B. melanostictus	AMNH 161135	DQ284324	FMNH 255309	DQ158317
B. viridis	AMNH 168402	DQ284297	TNHC (DMH89-21)	KJ532295
B. haematiticus	SIUC 7059	DQ284205	QCAZ 13215	DQ158302

Table S1: Sample and sequence information for all loci used in this analysis.
Part 2 of 3, continues on next page.

species	RAG1 ID	RAG1 GB	Rhod ID	Rhod GB
B. americanus	TNHC (DMH88-79)	KJ609650	TNHC 62701	FJ004273
B. houstonensis	TNHC (DMH88-3)	KJ609651	TNHC (DMH88-3)	KJ532265
B. hemiophrys	MVZ 137738	KJ609652	MVZ 137738	FJ004269
B. woodhousii	TNHC 60511	KJ609653	RNF 2417	DQ283875
B. terrestris	MVZ 223379	KJ609654	AMNH 168433	DQ283854
B. microscaphus	MVZ 223365	KJ609655	MVZ 223365	KJ532266
B. cognatus	MVZ 143048	KJ609656	MVZ 143048	KJ532267
B. speciosus	TNHC 60379	KJ609657	TNHC (AHP3496)	KJ532268
B. quercicus	MVZ 223370	KJ609658	MVZ 223370	KJ532269
B. punctatus	TNHC 58788	KJ609659	AMNH 168398	DQ283855
B. boreas	MVZ 142827	KJ609660	RNF2416	DQ283871
B. canorus	MVZ 142992	KJ609661	MVZ 142992	KJ532270
B. bocourti	MVZ 143367	KJ609662	MVZ 143367	KJ532271
B. alvarius	TNHC 61247	KJ609663	ATH499	DQ283933
B. occidentalis	UTA 34111	KJ609664	UTA 34111	KJ532272
B. valliceps	UTA 13097	KJ609665	UTA 13097	KJ532273
B. nebulifer	TNHC 62000	KJ609666	VogelQU5	EF372185
B. mazatlanensis	MVZ 132973	KJ609667	MVZ 132973	KJ532274
B. luetkenii	MVZ 207144	KJ609668 [$]	MVZ 207144	KJ532275
B. coccifer	KU 290030	KJ609669	KU 290330	KJ532276
B. canaliferus	UTA 34110	KJ609670	UTA 34110	KJ532277
B. marmoreus	UTA 13032	KJ609671	UTA 13032	KJ532278
B. marinus	KU 205236	KJ609672	MJH3678	DQ283789
B. schneideri	KU 289057	KJ609673	BB1224	DQ283791
B. poeppigii	USNM 268824	KJ609674	MNCN/ADN6174	HM159243
B. crucifer	ZUEC (DCC3392)	KJ609675	CHUNB 49567	HM159239
B. arenarum	AR305	DQ158354[$]	MACN 38639	AY844547
B. spinulosus	NB96-23	KJ609676	BB1032	DQ283775
B. regularis	AG47	KJ609677	SIH04	AY323745
B. maculatus	CAS (JV1677)	KJ609678	AMNH 163573	DQ284005
B. garmani	CAS 214829	KJ609679	CAS 214829	KJ532279
B. brauni	FMNH 251853	DQ158361[$]	RdS952	DQ284021
B. stomaticus	CAS 232071	KJ609680	CAS 232071	KJ532280
B. melanostictus	TNHC 59161	KJ609681	AMNH 161135	DQ283967
B. viridis	TNHC 56752	KJ609682	AMNH 168402	DQ283940
B. haematiticus	AG1	KJ609683	SIUC7059	DQ283861

Table S1: Sample and sequence information for all loci used in this analysis.
[$] Partial sequence.
Part 3 of 3, end of Table S1.

Primer Name	Primer Sequence(5' to 3')	Direction
RAG103Mod	TCKGARTGGAAGTTCAARCTGTT	Forward
RAGCWE220	GGAAAGAGAAGAARGCCACC	Forward
RAG182Rev	ATGATRCTCCAGCAGTTATGGC	Reverse
RAGCWE1100	TCCAAGCATAARGAAATCAAAGG	Forward
RAGCWE5prime	GGTTGGAAGATYTGCCTCCCWGTTATGG	Reverse
MartFL1Bufo	AGCTGTAGCCAGTACCAYAAMATG	Forward
RAGCWE2krev	TCRTGATCTGATTCATCRGCAAGC	Reverse
AMPF1mod	ACAGGKTAYGAYGAGAAGTTKGTGCG	Forward
AmpR1mod	AACTCKGCMGCRTTWCCRATGTC	Reverse
RAGCWE3prime	TGTGTAAAGCCAATGATGCTTCAAAAC	Reverse

Table S2: Primers used for amplification and sequencing of RAG1. Primers designed by D. C. Cannatella, C. W. Edwards, and G. B. Pauly, in some cases as slight modifications of primers from Chiari et al.(2004).

Barrier	# worse dam	# better dam
Fertility	9	5
Hatching	2	5
Metamorphosis	1	0

Table S3: Number of reciprocal crosses where *B. regularis* is the worse or better dam. Given the relatively high rate of mitochondrial evolution on the *regularis* / *maculatus* branch, the deterministic theory predicts that F1 offspring of *B. regularis* mothers will have relatively low viability.

Barrier	# worse dam	# better dam
Fertility	4	3
Hatching	1	3
Metamorphosis	1	0

Table S4: Number of reciprocal crosses where *B. maculatus* is the worse or better dam. Given the relatively high rate of mitochondrial evolution on the *regularis* / *maculatus* branch, the deterministic theory predicts that F1 offspring of *B. maculatus* mothers will have relatively low viability.

Files S2-S3

Available for download as .zip files at http://www.genetics.org/lookup/suppl/doi:10.1534/genetics.113.161133/-/DC1

File S2 Aligned sequences

File S3 R code for analyses